1073 K (800 °C) Isothermal Section of the Co-Al-V System

GUANGJING LIAO, FUCHENG YIN, YE LIU, and MANXIU ZHAO

The isothermal section of the Co-Al-V ternary system at 1073 K (800 °C) has been determined by means of X-ray diffraction and scanning electron microscopy coupled with energy-dispersive X-ray spectroscopy. Thirteen three-phase regions have been confirmed experimentally. A new ternary compound named 'T' phase (Al_2CoV) is found in this study which possesses a face-centered cubic (fcc) structure with a lattice parameter of 11.7224 Å. The T phase can be in equilibrium with Al_3V, Al_8V_5, α-V, Al_5Co_2, and AlCo. The maximum solubility of Al in Co_3V, σ-CoV, and CoV_3 is 5.6, 6.3, and 4 at. pct, respectively. The maximum solubility of Co in Al_3V, Al_8V_5, and α-V is 1.1, 2.5, and 24.9 at. pct, respectively. The maximum solubility of V in Al_9Co_2, $Al_{13}Co_4$, Al_3Co, Al_5Co_2, AlCo, and α-Co is 0.3, 0.2, 0.1, 2.1, 35.0, and 16.4 at. pct, respectively.

DOI: 10.1007/s11661-017-4137-3

I. INTRODUCTION

Ni-BASED alloys are the most widely used superalloys and are strengthened by a γ′ phase precipitated in the disordered fcc matrix phase (γ). Co-based alloys exhibit a better resistance to hot corrosion, but because of the lower strength compared with Ni-based superalloys, they have not found widespread usage.[1] However, Sato *et al*. discovered a new type of Co-based superalloy strengthened by a ternary compound, γ′ $Co_3(Al,W)$, which has great high-temperature strength.[2] Co-based alloys are thus regarded as the promising candidates for applications at high temperatures.[1,2] In adding elements to Co-based alloys, vanadium can play an important role in solution strengthening and precipitation strengthening. It enhances the matrix strength by forming a solid solution with Co[3] and by forming a carbide (or nitride) with a high hardness and high melting point in Co-based alloys.[4] In addition, it can refine crystal grains to improve the microhardness and wear resistance.[5] Aluminum is another important alloying element in Co-based alloys. Al can form a dense Al_2O_3 film which is able to improve the oxidation resistance and hot corrosion resistance of the alloy.[6] To understand the action mechanism and the related phase equilibrium of vanadium and aluminum in Co-based alloys at high temperature, the Co-Al-V isothermal section at 1073 K (800 °C) was determined experimentally in the present work.

II. LITERATURE DATA

In the Al-V binary system, two intermediate phases have been reported at 1073 K (800 °C): namely, Al_3V and Al_8V_5, which are line compounds.[7] However, Richter and Ipser[8] have reinvestigated the system and found that Al_3V and Al_8V_5 showed a small homogeneity range. Gong *et al*.[9] have carried out a thermodynamic reassessment of the system including the new results of Reference 7 in their optimization. In the Co-V system, three intermetallic compounds are present: Co_3V, σ-CoV, and CoV_3.[3] In 2003, a thermodynamic evaluation of the Co-V binary system was achieved by Bratberg and Sundman.[10] Many researchers have previously studied the Al-Co system.[11–15] Among the researchers, Massalski *et al*.[3] pointed out that there are five intermediate phases in the Al-Co system at 1073 K (800 °C): Al_9Co_2, Al_3Co, $Al_{13}Co_4$, Al_5Co_2, and AlCo. Mihalkovič *et al*.[14] applied first-principles calculations to compare the cohesive energies of both proven and hypothetical structures. They confirmed the experimentally established phase diagram in every detail except near $Al_{13}Co_4$. However, the homogeneity range of the AlCo phase in the central part of the Al-Co phase diagram has not been well established. Stein *et al*.[15]

GUANGJING LIAO, FUCHENG YIN, and MANXIU ZHAO are with the School of Material Science and Engineering Xiangtan University, Xiangtan, 411105, Hunan People's Republic of China, and also with Key Laboratory of Materials Design and Preparation Technology of Hunan Province, Xiangtan University, Xiangtan, 411105, Hunan People's Republic of China. Contact e-mail: fuchengyin@xtu.edu.cn YE LIU is with School of Material Science and Engineering, Xiangtan University, also with Key Laboratory of Materials Design and Preparation Technology of Hunan Province, Xiangtan University, and also with the State Key Laboratory of Powder Metallurgy, Central South University, Changsha, 410083, Hunan People's Republic of China.

Manuscript submitted January 19, 2017.
Article published online May 15, 2017

established the Al-rich phase boundary of the AlCo phase and the Co-rich boundary of the Al_5Co_2 phase experimentally, and re-assessed the phase diagram based on the CALPHAD method. All crystallographic parameters for the binary compounds related to the present work are listed in Table I. However, the Co-Al-V ternary system has never been reported. The binary systems Al-V,[8] Co-V,[3] and Al-Co[15] are used as the boundary conditions for the present ternary system.

III. EXPERIMENTAL METHODS

In all, 25 alloys were prepared to determine the equilibrium phases in the Co-Al-V system. Their compositions are shown in Table II. The alloys with an aluminum content of less than 60 at. pct were prepared from high-purity Co chips (99.99 wt pct), Al grains (99.99 wt pct), and V grains (99.99 wt pct) by arc melting under an Ar atmosphere. Each alloy ingot was melted four times and turned over between melting to achieve uniformity. Each alloy was placed into a corundum crucible and then sealed in an evacuated quartz tube. To prevent excessive loss of aluminum in the arc, the other parts of the alloys with higher aluminum content used another method for smelting the alloy. These alloys were prepared from high-purity Co powders (99.99 wt pct), Al grains (99.99 wt pct), and V powders (99.99 wt pct) because the Co and V powders can be mixed more easily to uniformity than Co chips and V grains. The raw materials were mixed in a corundum crucible and then sealed in an evacuated quartz tube. To promote melting, the sealed specimens were heated to 1373 K (1100 °C) and held at that temperature for 72 hours, after which they were quenched in water. The quenched specimens were then resealed in an evacuated quartz tube. All specimens were annealed at 1073 K (800 °C) for 1440 hours, followed by quenching in water.

All annealed alloys were prepared in the conventional way for metallographic examination. Microstructural observations and compositional analyses of various phases were carried out using an optical microscope and a JSM-6360LV scanning electron microscope (SEM) coupled with energy-dispersive X-ray spectroscopy (EDS) after etching by a 20 wt pct HF, 20 wt pct HNO_3, and 60 wt pct H_2O_2 solution. The constituent phases of the alloys were further ascertained by analyzing X-ray diffraction (XRD) patterns generated by a Rigaku Ultima IV diffractometer, operating with Cu-Kα radiation. The compositions reported in this paper were obtained from the average value of at least five measured results.

IV. RESULTS AND DISCUSSION

All phases found in the alloys are listed in Table II, as are the chemical compositions of those phases. Please note that Al is in the liquid state at 1073 K (800 °C), so it was marked as "L-Al" in the present work.

According to the SEM–EDS analysis results of alloys A1, A2, A3, and A4 as shown in Figure 1, we have found four three-phase regions near the Al-rich side of the 1073 K (800 °C) isothermal section of the Co-Al-V system: $Al_9Co_2 + Al_3V + L\text{-}Al$, $Al_9Co_2 + Al_3V + Al_{13}Co_4$, $Al_{13}Co_4 + Al_3V + Al_3Co$, and $Al_3Co + Al_3V + Al_5Co_2$ three-phase equilibrated regions. Figure 1(a) shows the microstructure of alloy A1. SEM–EDS analysis indicated that the L-Al phase is located around the Al_9Co_2 and Al_3V grains. The Al_3V phase is a bit darker than the Al_9Co_2 phase. The solubility of V in Al_9Co_2 reaches 0.3 at. pct. The microstructure of alloy A2 is shown in Figure 1(b). SEM–EDS analysis indicates that the L-Al phase is absent. Al_3V, Al_9Co_2, and $Al_{13}Co_4$ are coexistent. The V solubility in Al_9Co_2 and $Al_{13}Co_4$ is 0.2 at. pct. Figure 1(c) shows the microstructure of alloy A3, indicating that Al_3V, Al_3Co, and $Al_{13}Co_4$ phases coexist in this alloy. Because of the low content of V in this alloy, the proportion of Al_3V is much less than that of $Al_{13}Co_4$ and Al_3Co. Figure 1(d) shows the microstructure of alloy A4 containing the following phases: Al_3V, Al_5Co_2, and the gray Al_3Co which contains 0.1 at. pct V. The Al_3V phase is a bit darker than the Al_5Co_2 phase. The solubility of Co reaches 1.1 at. pct in Al_3V. Figure 2 shows the XRD patterns of alloys A1, A2, A3, and A4, which confirms that these alloys are located in the $Al_9Co_2 + Al_3V + L\text{-}Al$, $Al_9Co_2 + Al_3V + Al_{13}Co_4$, $Al_{13}Co_4 + Al_3V + Al_3Co$, and $Al_3Co + Al_3V + Al_5Co_2$ three-phase equilibrium

Table I. Crystallographic Parameters for Binary Compounds Required in the Co-Al-V Ternary System

Compound	Person Symbol	Space Group	Lattice Parameters, nm			Refs.
			a	b	c	
Al_8V_5	cI52	*I*3*m*	0.9235	—	—	7, 8
Al_3V	tI8	*I*4/*mmm*	0.3780	—	—	7, 8
Al_9Co_2	mP22	$P2_1/c$	10.1490	6.2905	8.5560	16
$Al_{13}Co_4$	oP102	*Cm*	15.1830	8.1220	12.3400	16
Al_3Co	mC656	C_2/m	16.9890	4.0980	7.4780	17
Al_5Co_2	hP28	$P6_3/mmc$	7.6560	7.5932	—	16
AlCo	cP2	*Pm*-3*m*	2.8630	—	—	16
Co_3V	hP24	*Pm*3*n*	0.4681	—	—	3, 16
σ-CoV	tP30	$P4_2/mnm$	0.8834	0.8834	0.4587	3, 16
CoV_3	cP8	*Pmm*	0.3557	—	—	3, 16

Table II. Composition of Alloys and Phases in the Co-Al-V Ternary System at 1073 K (800 °C) (At. Pct)

Alloy No.	Designed Composition	Phase	Compositions (At. Pct) Co	Al	V
A1	Co5-Al85-V10	L-Al	1.3	98.5	0.2
		Al_3V	0.5	74.8	24.7
		Al_9Co_2	18.2	81.5	0.3
A2	Co13-Al77-V10	Al_3V	0.7	74.6	24.7
		Al_9Co_2	18.2	81.6	0.2
		$Al_{13}Co_4$	23.9	75.9	0.2
A3	Co24-Al75-V1	Al_3V	1.0	74.2	24.8
		$Al_{13}Co_4$	24.2	75.8	0
		Al_3Co	26.3	73.7	0
A4	Co22-Al73-V5	Al_3V	1.1	73.8	25.1
		Al_3Co	26.3	73.6	0.1
		Al_5Co_2	27.6	72.4	0
A5	Co10-Al60-V30	Al_3V	0.6	73.6	25.8
		Al_8V_5	2.5	61.3	36.2
		T	23.4	51.8	24.8
A6	Co20-Al60-V20	Al_3V	0.8	73.7	25.5
		Al_5Co_2	28.7	69.2	2.1
		T	24.6	53.7	21.7
A7	Co30-Al60-V10	Al_5Co_2	29.2	69.3	1.5
		AlCo	44.3	50.5	5.2
		T	25.5	53.2	21.2
A8	Co3-Al47-V50	Al_8V_5	1.1	60.5	38.4
		α-V	3.2	41.3	55.6
		T	23.1	50.6	26.3
A9	Co30-Al46-V24	α-V	5.0	38.0	57.0
		T	24.4	47.9	27.6
		AlCo	42.6	47.0	10.4
A10	Co24-Al4-V72	σ-CoV	26.6	4.0	69.5
		CoV_3	23.7	1.9	74.4
		α-V	18.1	10.0	71.9
A11	Co34-Al16-V50	α-V	~24.9	~13.9	~61.2
		AlCo	~43.9	~22.6	~33.5
		σ-CoV	~31.2	~6.3	~62.5
A12	Co54-Al10-V36	AlCo	53.0	15.1	31.9
		σ-CoV	53.8	2.0	44.2
		Co_3V	66.9	2.4	30.7
A13	Co73-Al10-V17	AlCo	63.3	23	13.7
		Co_3V	75.2	5.6	19.2
		α-Co	76.9	6.7	16.4
A14	Co30-Al38-V32	α-V	8.8	32.2	59.0
		AlCo	40.7	41.2	18.1
A15	Co30-Al29-V41	α-V	~16.0	~22.9	~61.1
		AlCo	~40.8	~33.2	~26.0
A16	Co20-Al4-V76	α-V	14.9	6.9	78.1
		CoV_3	24.3	1.0	74.7
A17	Co23-Al10-V67	α-V	21.6	12.3	66.1
		σ-CoV	26.8	5.3	67.9
A18	Co45-Al10-V45	σ-CoV	44.2	5.3	50.5
		AlCo	46.5	18.5	35.0
A19	Co50-Al10-V40	AlCo	50.2	15.9	33.9
		σ-CoV	48.9	3.9	47.2
A20	Co63-Al10-V27	AlCo	58.4	15.9	25.7
		Co_3V	68.7	3.9	27.4
A21	Co69-Al10-V21	Co_3V	72.7	5.6	21.7
		AlCo	61.4	18.3	20.3
A22	Co79-Al10-V11	AlCo	63.4	26.0	10.6
		α-Co	82.3	6.2	11.5
A23	Co85-Al10-V5	AlCo	61.8	32.4	5.8
		α-Co	87.9	6.6	5.5

Table II. continued

Alloy No.	Designed Composition	Phase	Compositions (At. Pct) Co	Al	V
A24	Co80-Al3-V17	Co_3V	76.4	4.1	19.5
		α-Co	84.0	2.7	13.3

The uncertainty of the phase compositions is less than ±0.5 at. pct.

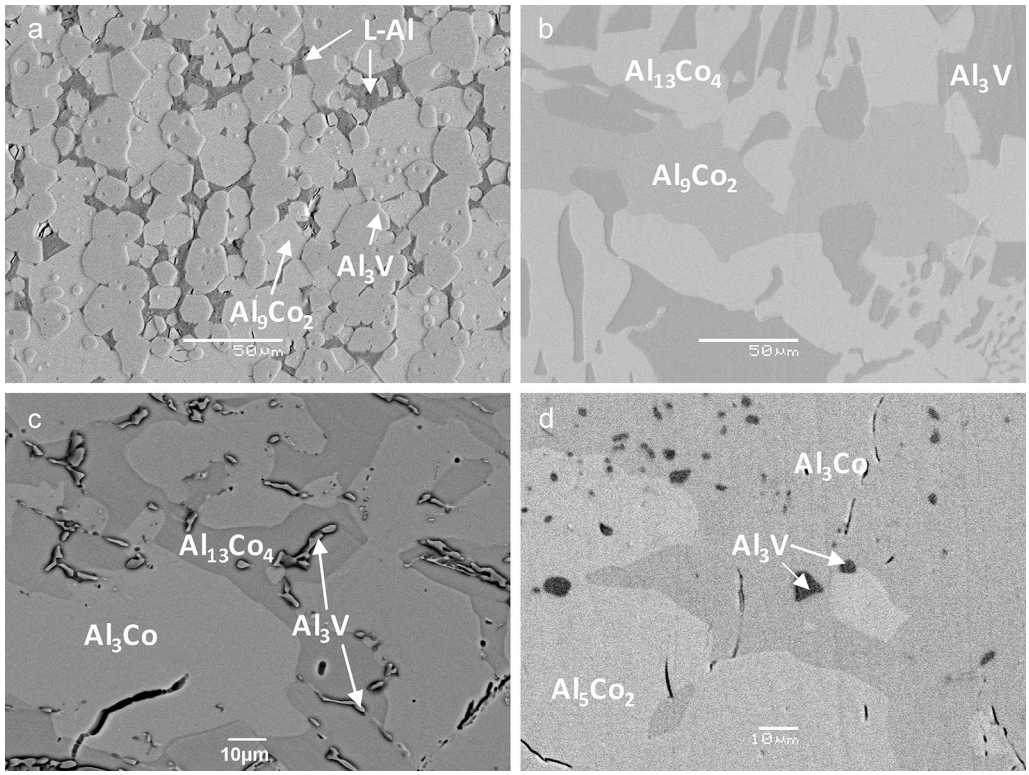

Fig. 1—SEM images of different alloys near the Al-rich side. (*a*) alloy A1, $Co_2Al_9 + Al_3V + L\text{-}Al$; (*b*) alloy A2, $Al_9Co_2 + Al_3V + Al_{13}Co_4$; (*c*) alloy A3, $Al_{13}Co_4 + Al_3V + Al_3Co$; and (*d*) alloy A4, $Al_3Co + Al_3V + Al_5Co_2$.

regions, respectively. When cooled from 1073 K (800 °C) to room temperature, L-Al became α-Al phase, so the XRD patterns of alloy A1 contains α-Al phases.

A new ternary compound, named the 'T' phase (Al_2CoV), containing 21.2-27.6 at. pct V and 47.9-53.7 at. pct Al, was found in this study. Alloys A5, A6, A7, A8, and A9 contain the T phase. Based on the SEM–EDS analysis, the T phase is confirmed to be in equilibrium with Al_3V, Al_8V_5, α-V, Al_5Co_2, and AlCo. As shown in Figure 3(a), the microstructure of alloy A5 clearly indicates the existence of three phases: the bright bulk T phase, convex gray Al_8V_5, and the Al_3V matrix. The solubility of Co in Al_8V_5 is 2.5 at. pct. Figure 3(b) shows the backscattered electron (BSE) micrograph of alloy A6, which indicates that alloy A6 is located in the $T + Al_5Co_2 + Al_3V$ three-phase equilibrium region. The Al_5Co_2 phase contains 2.1 at. pct V, and the T phase contains 21.7 at. pct V, and 53.7 at. pct Al. Figure 3(c) shows the BSE micrograph of alloy A7, which indicates that the AlCo, T, and Al_5Co_2 phases coexist. The solubility of V and Al in T is 21.2 and 53.2 at. pct, respectively. Figure 4(d) shows the microstructure of alloy A8 with the following phases: the gray bulk α-V,

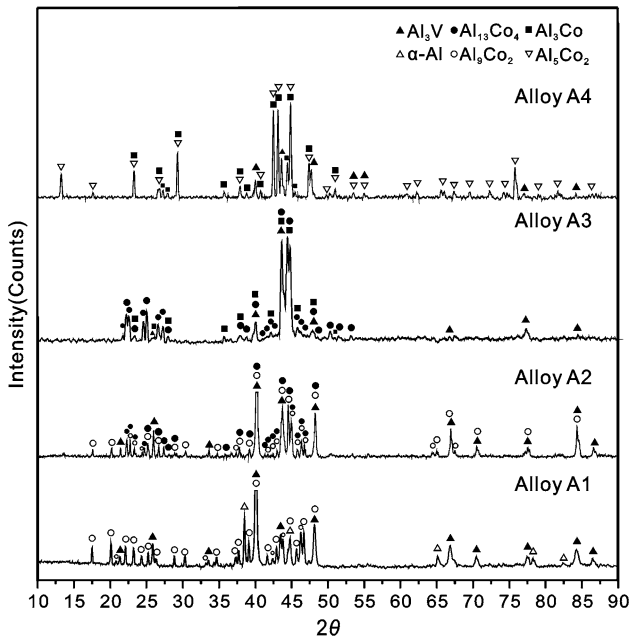

Fig. 2—XRD patterns of alloys near the Al-rich side.

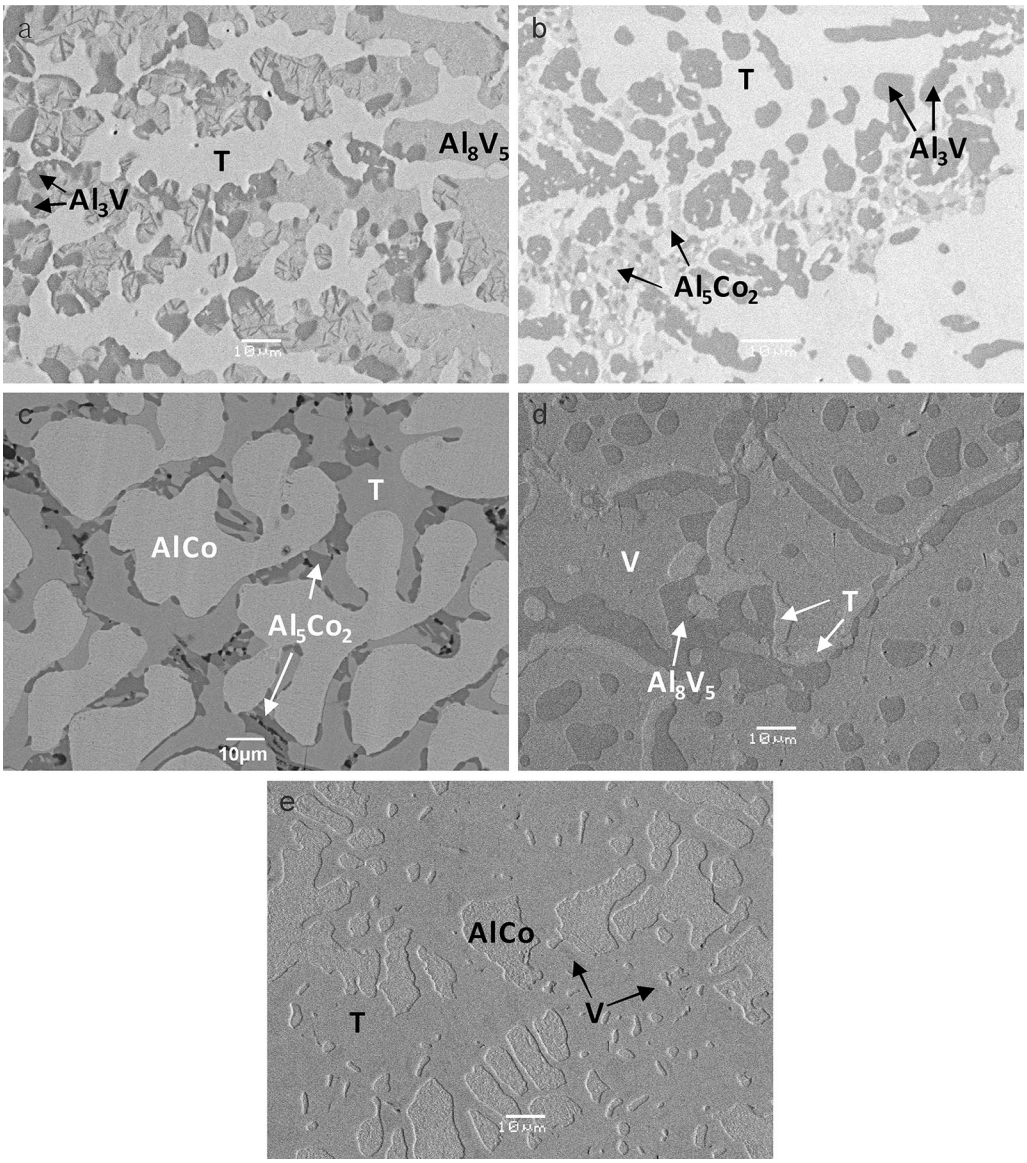

Fig. 3—The typical microstructures of different alloys around the T phase. (*a*) alloy A5, $T + Al_3V + Al_8V_5$; (*b*) alloy A6, $T + Al_3V + Al_5Co_2$; (*c*) alloy A7, $T + AlCo + Al_5Co_2$; (*d*) alloy A8, $T + \alpha\text{-}V + Al_8V$; and (*e*) alloy A9, $T + AlCo + \alpha\text{-}V$.

dark-gray Al_8V_5, and light-gray T. The microstructure of alloy A9 is shown in Figure 3(e). SEM–EDS analysis indicates that the AlCo matrix contains α-V and T phases. Because the α-V phase is very similar in contrast to the T phase, it is not easy to identify. In this alloy, the T phase contains 26.7 at. pct V and 47.9 at. pct Al. Figure 4 shows the XRD patterns of alloys A5, A6, A7, A8, and A9. These patterns clearly indicate that these alloys are in the $T + Al_3V + Al_8V_5$, $T + Al_3V + Al_5Co_2$, $T + AlCo + Al_5Co_2$, $T + \alpha\text{-}V + Al_8V$, and $T + AlCo + \alpha\text{-}V$ three-phase equilibrium states, respectively. It is remarkable that the diffraction peaks of the α-V phase of alloy A8 move to the left side of the standard α-V phase XRD pattern. This is because Al atoms occupy the lattice points of V atoms without changing the crystal structure of the α-V phase and thus form a solid solution.

To identify the crystal structure of the T phase, alloy S1 with nominal composition Co25Al50V25 was prepared with the intent of obtaining a pure T phase. The alloy was annealed at 1073 K (800 °C) for 1440 h. Figure 5 presents the XRD patterns of alloy S1, which shows that the major phase is the T phase. From Figure 5, we can see there are four lower peaks of the AlCo phase and three of the α-V phase. The XRD result shows the real composition of alloy S1 located in the $T + AlCo + \alpha\text{-}V$ three-phase-equilibrated field, which results from the loss of aluminum during the smelting process. By means of Jade 6, the refinement results of

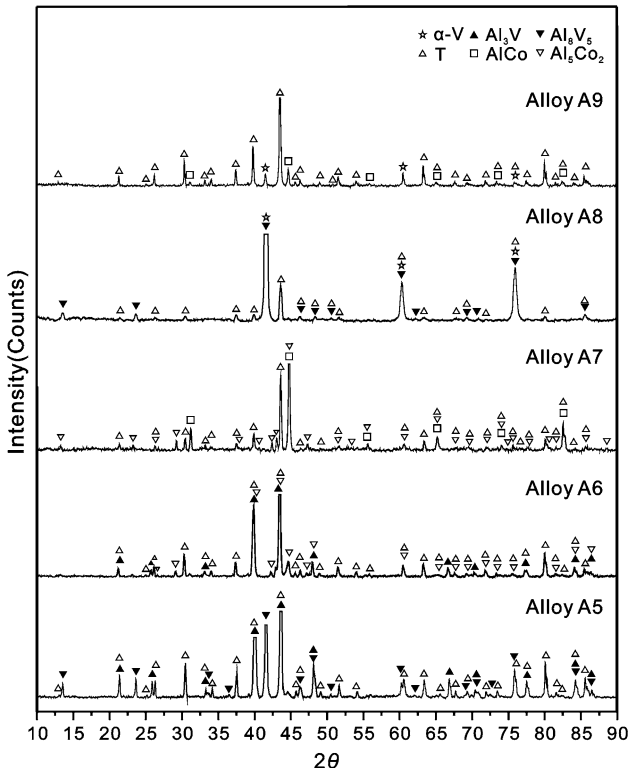

Fig. 4—XRD patterns of alloys near the T phase.

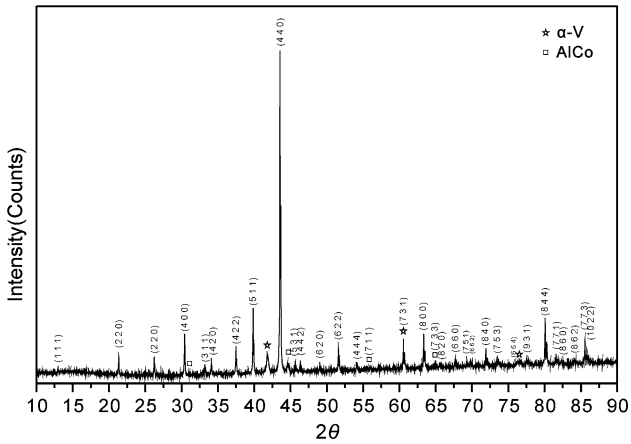

Fig. 5—XRD patterns of alloy S1 (Co25Al50V25).

the XRD confirmed that the T phase belongs to a fcc structure with a lattice parameter of 11.7224 Å. The index of the T phase is labeled in Figure 5.

On the basis of the SEM–EDS analysis of alloys A10, A11, A12, and A13 as shown in Figure 6, we have also found that four three-phase regions exist near the Co-V-rich side of the 1073 K (800 °C) isothermal section in the Co-Al-V system. They are $CoV_3 + \alpha$-V + σ-CoV, AlCo + α-V + σ-CoV, Co_3V + AlCo + σ-CoV, and Co_3V + α-Co + AlCo three-phase equilibrated regions. The microstructure of alloy A10 is shown in Figure 6(a). SEM–EDS analysis indicates that the α-V and CoV_3 phases coexist in the σ-CoV matrix. The CoV_3 phase is very similar in contrast to σ-CoV, but after etching, the σ-CoV phase has been more deeply corroded. In this alloy, the Al solubility in CoV_3 is 1.9 at. pct and the Co solubility in α-V is 23.7 at. pct. Figure 6(b) reveals the microstructure of alloy A11. Due to the fine microstructure, the EDS results are not very accurate. SEM–EDS analysis indicates that the σ-CoV phase, which contains about 6.3 at. pct Al, shows the best corrosion resistance. The sunken microstructure is AlCo, and the remaining phase is α-V, which contains about 24.9 at. pct Co. Figure 6(c) shows the BSE micrograph of alloy A12, wherein three different phases can be observed. The gray whiskers appertain to the Co_3V phase and the bright regions represent σ-CoV phases. The matrix is in the AlCo phase. The solubility of V in AlCo is 31.9 at. pct. Figure 6(d) shows the microstructure of alloy A13, containing three phases: the gray granular Co_3V, which contains 5.6 at. pct Al, the convex gray α-Co, and the sunken AlCo. The solubility of V reaches 16.4 at. pct in α-Co. Figure 7 shows the XRD patterns of alloys A10, A11, A12, and A13, which confirms that these alloys are located in the CoV_3 + V + σ-CoV, AlCo + V + σ-CoV, Co_3V + AlCo + σ-CoV, and Co_3V + α-Co + AlCo three-phase equilibrium regions, respectively. It is worth noting that the diffraction peaks of the α-V phase of alloy A10 move to the right side, which can be attributed to the fact that Co atoms occupy the lattice points of V atoms without changing the crystal structure of the α-V phase and form a solid solution.

The alloys mentioned above are in a three-phase equilibrium state. The alloys in a two-phase equilibrium state are not detailed herein, but their compositional details are listed in Table II. Based on the above results and binary systems in the relevant literature,[3,8,15] the 1073 K (800 °C) isothermal section of the Co-Al-V ternary system is established, as shown in Figure 8. There are thirteen three-phase regions which have been confirmed experimentally. A new ternary compound T phase was found, which is in equilibrium with Al_3V, Al_8V_5, α-V, Al_5Co_2, and AlCo. The AlCo phase regions are extraordinarily large and can be in equilibrium with all of the phases near the Co-V-rich side, except for CoV_3.

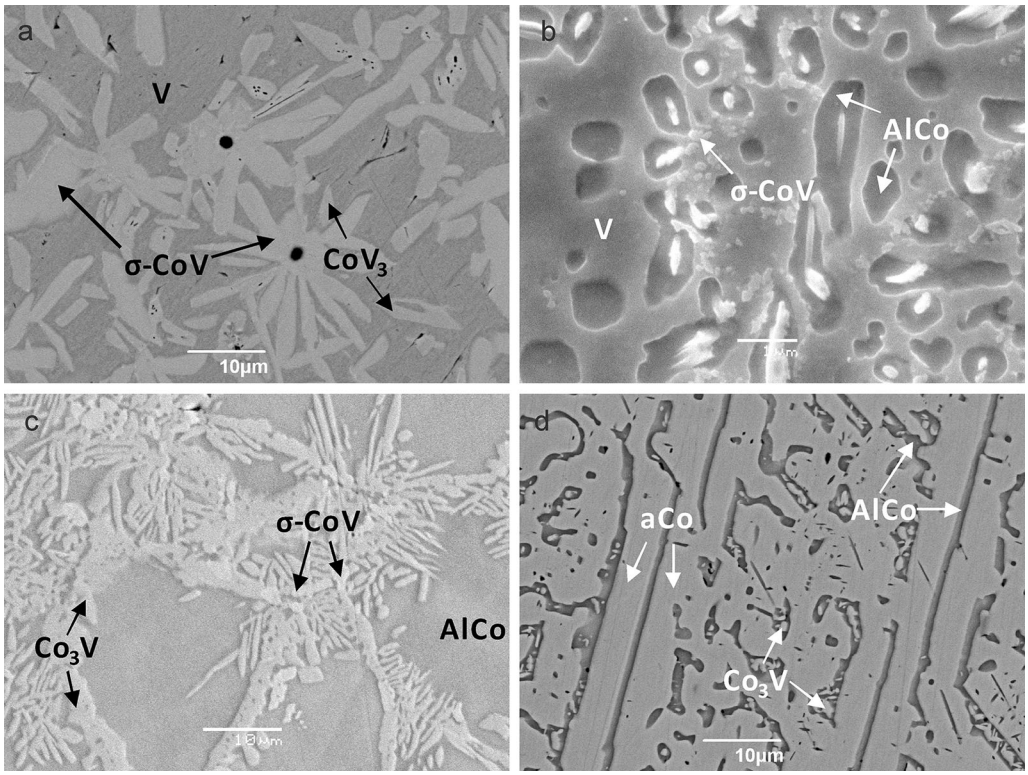

Fig. 6—Microstructures of different alloys near the Co-V-rich side. (*a*) alloy A10, $CoV_3 + \alpha\text{-V} + \sigma\text{-CoV}$; (*b*) alloy A11, $AlCo + \alpha\text{-V} + \sigma\text{-CoV}$; (*c*) alloy A12, $Co_3V + AlCo + \sigma\text{-CoV}$; and (*d*) alloy A13, $Co_3V + \alpha\text{-Co} + AlCo$.

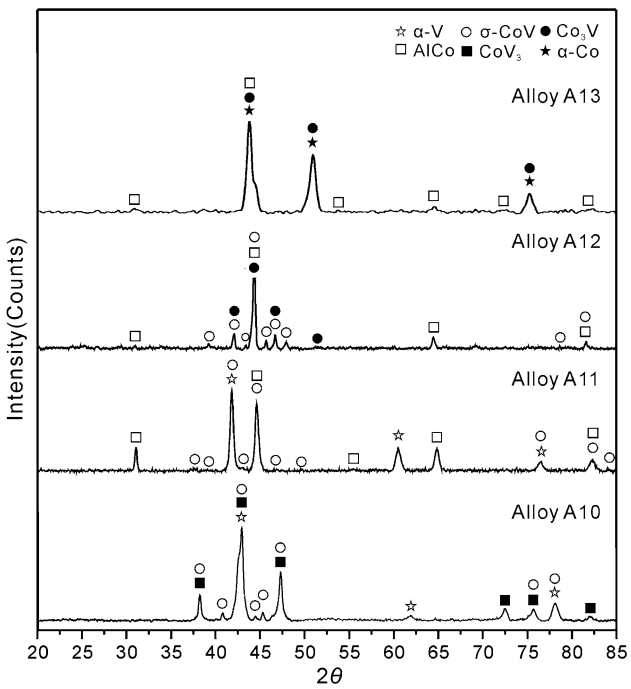

Fig. 7—XRD patterns of alloys near the Co-V-rich side.

V. CONCLUSIONS

1. The isothermal section of the Co-Al-V system at 1073 K (800 °C) has been determined by means of SEM/EDS and XRD techniques.
2. A new ternary compound T phase (Al_2CoV) is confirmed which possesses a fcc structure with a lattice parameter of 11.7224 Å. The T phase can be in equilibrium with Al_3V, Al_8V_5, α-V, Al_5Co_2, and AlCo.
3. The AlCo phase regions are extraordinarily large and can be in equilibrium with all of the phases near the Co-V-rich side except for the CoV_3 phase.
4. There are thirteen three-phase regions: $Al_9Co_2 + Al_3V +$ L-Al, $Al_9Co_2 + Al_3V + Al_{13}Co_4$, $Al_{13}Co_4 + Al_3V + Al_3Co$, $Al_3Co + Al_3V + Al_5Co_2$, $T + Al_3V + Al_8V_5$, $T + Al_3V + Al_5Co_2$, $T + AlCo + Al_5Co_2$, $T + \alpha\text{-V} + Al_8V$, $T + AlCo + \alpha\text{-V}$, $CoV_3 + \alpha\text{-V} + \sigma\text{-CoV}$, $AlCo + \alpha\text{-V} + \sigma\text{-CoV}$, $Co_3V + AlCo + \sigma\text{-CoV}$, and $Co_3V + \alpha\text{-Co} + AlCo$ in the Co-Al-V isothermal section at 1073 K (800 °C).
5. The maximum solubility of Al in Co_3V, σ-CoV, and CoV_3 is 5.6, 6.3, and 4 at. pct, respectively. The maximum solubility of Co in Al_3V, Al_8V_5, and α-V is 1.1, 2.5, and 24.9 at. pct, respectively. The maximum solubility of V in Al_9Co_2, $Al_{13}Co_4$, Al_3Co, Al_5Co_2, AlCo, and α-Co is 0.3, 0.2, 0.1, 2.1, 35.0, and 16.4 at. pct, respectively.

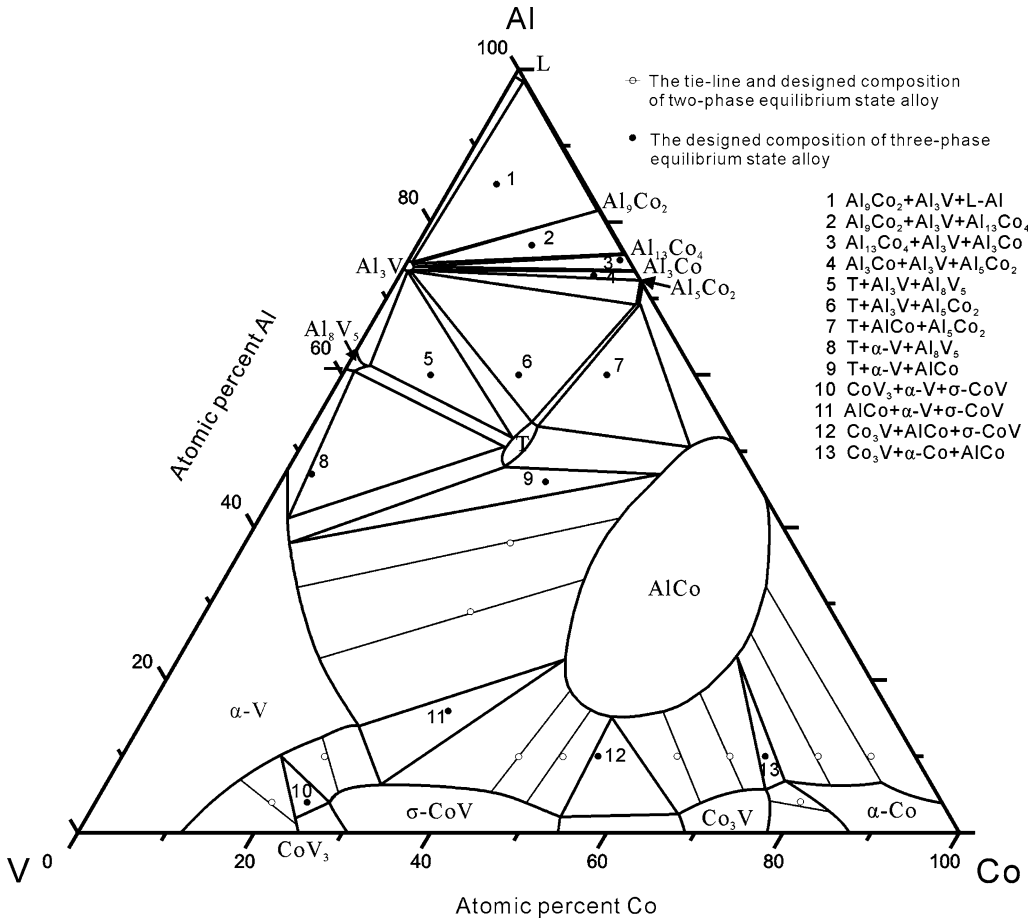

Fig. 8—The 1073 K (800 °C) isothermal section of the Co-Al-V ternary system.

ACKNOWLEDGMENTS

The authors wish to thank Dr. L.J. Gong for identifying the T phase crystal structure. This work was supported by the National Natural Science Foundation of China (No. 51471141 and No. 51471140), Scientific Research Fund of Hunan Provincial Science and Technology Department (No. 2016JC2005), and the 2015 opening subject of State Key Laboratory of Powder Metallurgy.

REFERENCES

1. C.H.T. Sims, N.S. Stoloff, and W.C. Hagel: *Superalloys II*, Wiley, New York, 1987, p. 135.
2. J. Sato, T. Omori, K. Oikawa, I. Ohnuma, R Kainuma, and K Ishida: *Science*, 2006, vol. 312, pp. 90–91.
3. T.B. Massalski, H. Okamoto, and P.R. Subramanian: L. Kacprzak (Eds.), *Binary Alloy Phase Diagrams*, 2nd ed., ASM International, Metals Park, OH, 1990.
4. W. Betteridge: *Cobalt and its alloys*, Wiley, New York, E. Horwood, 1982, pp. 63–79.
5. L. Ding, S.S. Hu, X.M. Quan, and J.Q. Shen: *J. Alloys Compd.*, 2016, vol. 659, pp. 8–14.
6. J.-W. Lee and Y.-C. Kuo: *Surf. Coat. Technol.*, 2005, vol. 200 (5–6), pp. 1225–30.
7. J.L. Murray: *Bull. Alloy PhaseDiagr.*, 1989, vol. 10, pp. 351–57.
8. K.W. Richter and H. Ipser: *Z. Metallkd.*, 2000, vol. 91, pp. 383–88.
9. W.P. Gong, Y. Du, B.Y. Huang, R. Schmid-Fetzer, C.F. Zhang, and H. Xu: *Z. Metallkd.*, 2004, vol. 95 (11), pp. 978–86.
10. J. Bratberg and B. Sundman: *J. Phase Equilib.*, 2003, vol. 24 (6), pp. 495–503.
11. P. Villars, K. Cenzual, J.L.C. Daams, F. Hulliger, and H. Okamoto: K. Osaki (Eds.), Pauling File, Distributed by ASM International, Materials Park, OH.
12. B. Grushko, R. Wittenberg, K. Bickmann, and C. Freiburg: *J. Alloys Compd.*, 1996, vol. 233, pp. 279–87.
13. T. Gödecke and M. Ellner: *Z. Metallkd.*, 1996, vol. 87, pp. 854–64.
14. M. Mihalkovič and M. Widom: *Phys. Rev. B*, 2007, vol. 75, pp. 014207-1–014207-10.
15. F. Stein, C. He, and N. Dupin: *Intermetallics*, 2013, vol. 39, pp. 58–68.
16. P. Villars and L.D. Calvert: *Pearson's Handbook of Crystallographic Data for Intermetallic Phase*, 2nd ed., ASM International, Materials Park, OH, 1997.
17. C.H. Hu and X.Z. Li: *J. Alloys Compd.*, 2009, vol. 473, pp. 25–27.